An asymmetry of the electron foreshock due to the strahl

M. P. Pulupa,[1] S. D. Bale,[1,2] and C. Salem[1]

[1] We investigate statistically the dependence of electron foreshock Langmuir wave activity on the properties of the upstream electron distribution function, using wave and electron measurements from the *Wind* spacecraft. We find that the presence of a strong strahl beam in the upstream solar wind leads to a significant increase in the occurrence of Langmuir wave activity in the sunward wing of the electron foreshock, generating an asymmetry in the foreshock between the sunward and anti-sunward wings. This asymmetry of electrostatic wave occurrence is likely to be reflected in the radio emission properties of the two foreshock wings. The mechanism behind the asymmetry was first postulated in the context of the Venus foreshock, and may be relevant to recent observations of Langmuir wave activity in solar wind magnetic holes. Furthermore, the likely absence of a strahl-related enhancement at fast forward interplanetary shocks points out a key difference between the physics of electron acceleration at interplanetary shocks and bow shocks. **Citation:** Pulupa, M. P., S. D. Bale, and C. Salem (2011), An asymmetry of the electron foreshock due to the strahl, *Geophys. Res. Lett.*, *38*, L14105, doi:10.1029/2011GL048029.

1. Introduction

[2] The electron foreshock is the region, upstream of the quasiperpendicular bow shock and magnetically connected to the shock, where the upstream particle population is dominated by reflected solar wind electrons. These electrons, when accelerated back into the solar wind, form a beam and generate electrostatic Langmuir wave activity, which is then mode converted to radio emission at the plasma frequency and its harmonics. Observations of electron beams and associated wave activity in this region have been made for many decades [*Filbert and Kellogg*, 1979; *Anderson et al.*, 1979; *Fitzenreiter et al.*, 1996; *Larson et al.*, 1996; *Malaspina et al.*, 2009].

[3] Theoretical models of electron acceleration based on conservation of the electron adiabatic invariant have been successful in explaining the general characteristics of the upstream electron population, including the presence of an energy-dependent loss cone and bump-on-tail electron velocity distribution functions (eVDFs) [*Wu*, 1984; *Leroy and Mangeney*, 1984; *Cairns*, 1987; *Krauss-Varban et al.*, 1989; *Yuan et al.*, 2007]. Stochastic growth theory (SGT) [*Robinson*, 1992] describes the growth of beam-driven Langmuir waves and is consistent with observed wave activity [*Cairns and Robinson*, 1999]. A recent quantitative model [*Kuncic et al.*, 2004] incorporates the complete process of electron acceleration, beam-driven stochastic wave growth, and mode conversion of Langmuir waves to electromagnetic radio waves. Using this model, wave power and radio emissivity can be computed over the entire spatial range of the electron foreshock. However, up to this point the seed population of solar wind electrons has been modeled using a function which does not fully describe each component of the eVDF. This letter will demonstrate that a complete description of the upstream eVDF, in particular one which includes a realistic strahl, is crucial to understanding the structure of the electron foreshock.

[4] The solar wind eVDF is made up of several distinct components. The thermal core of the distribution makes up most of the number density of the electron distribution. However, since the positive cross shock potential which exists across the terrestrial bow shock is typically higher than the core electron temperature [*Kuncic et al.*, 2002; *Lefebvre et al.*, 2007], core electrons tend to be drawn into the downstream region of the shock, leaving the suprathermals to form the reflected electron beams which drive foreshock activity.

[5] The relevant suprathermal eVDF components are the halo and the strahl [*Pilipp et al.*, 1987]. The halo is well represented by a bi-Kappa distribution [*Maksimovic et al.*, 1997]. The strahl is a field-aligned beam-like feature propagating away from the sun and is thought to be the remnant of the coronal electron population. The relative contribution of the halo and strahl to the total electron density wax and wane respectively with increasing radial distance from the sun [*Maksimovic et al.*, 2005; *Štverák et al.*, 2009]. This relationship, as well as the fact that the two populations exist at similar energies, supports the theory that the strahl population gradually evolves into the halo, possibly due to scattering of strahl electrons by a wave-particle interaction [*Vocks et al.*, 2005].

[6] The electron foreshock is divided into two wings, one on either side of the point where the IMF is tangent to the shock. In this paper, the wings are designated the "sunward" and "anti-sunward" wings (Figure 1). The incident population (that is, the electrons that will be reflected by the shock) on the sunward side consists of electrons propagating *away* from the sun, while the incident population on the anti-sunward side consists of electrons which are propagating *towards* the sun. Foreshock beams generated in the sunward wing of the foreshock therefore originate from incident strahl and halo electrons, while foreshock beams generated in the anti-sunward wing originate from halo electrons alone.

[7] The asymmetry of the electron foreshock wings has previously been studied using the technique of statistical imaging. A strong asymmetry was found in the Venus electron foreshock [*Crawford et al.*, 1998, Plate 1]. The

[1]Space Sciences Laboratory, University of California, Berkeley, California, USA.
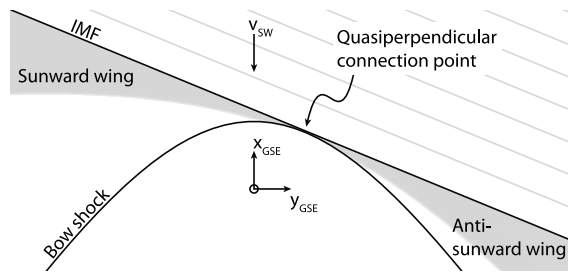[2]Physics Department, University of California, Berkeley, California, USA.

Figure 1. The electron foreshock (shown in gray) is divided into a sunward and anti-sunward wing. The incident suprathermal population on the sunward side consists of halo and strahl electrons, while the incident suprathermal population on the anti-sunward side contains only halo electrons.

authors proposed two explanations for the observed asymmetry: (1) differences in local shock strength at the acceleration point and (2) anisotropy of the upstream eVDF, as described above and as shown in Figure 7 of *Crawford et al.* [1998]. However, similar studies in the terrestrial electron foreshock did not conclusively observe such asymmetries [*Greenstadt et al.*, 1995; *Kasaba et al.*, 2000].

[8] The results presented here will demonstrate that the sunward/anti-sunward asymmetry does indeed exist in the terrestrial electron foreshock, and will also demonstrate directly the dependence of the asymmetry on the solar wind eVDF. In the final section, we will briefly discuss possible reasons why this effect was not reported by previous studies.

2. Observations

[9] During the first half of 1996, the *Wind* spacecraft made several Earth orbits with apogee locations ahead of the bow shock near the Sun-Earth line. These orbits avoided the ion foreshock region located farther downstream at the quasiparallel bow shock, and therefore offer an excellent opportunity for dedicated study of the electron foreshock.

[10] The interval selected for this study begins on 15 March 1996 and ends on 24 May 1996. On March 15th, *Wind* was located approximately 120 R_E upstream of the shock and was travelling towards the Earth. *Wind* then made three inbound/outbound crossing pairs of the shock and two complete orbits, with apogees of approximately 85 R_E. On May 24th, the spacecraft was traveling outbound once more, at approximately 130 R_E.

[11] The wave observations used in this study come from the *Wind*/WAVES instrument [*Bougeret et al.*, 1995], and the solar wind plasma parameters and electron pitch angle distributions are measured by the *Wind*/3DP instrument suite [*Lin et al.*, 1995].

[12] The 3DP SST Foil electron detector and the *Wind*/WAVES RAD1 and RAD2 radio receivers were used to inspect the study interval for the velocity dispersed electrons and drifting radio signals which signify solar electron events associated with *in situ* Langmuir waves [*Ergun et al.*, 1998]. Because solar activity was at a minimum in 1996, only a few weak Type III radio bursts were observed, and none were associated with *in situ* velocity dispersed electrons or Langmuir waves. Therefore, the observed Langmuir waves during this interval are exclusively the results of foreshock electron beams.

[13] In this study, Langmuir waves are detected algorithmically by comparing the relatively low power in the quasi-thermal plasma line [*Meyer-Vernet and Perche*, 1989] to the intense enhancement near the plasma line during periods of Langmuir wave activity. The algorithm records a wave when the power near the plasma line is a factor of 10 greater than the background thermal noise. This method was previously used to detect Langmuir waves upstream of interplanetary (IP) shocks and is described fully by *Pulupa et al.* [2010].

[14] During the study interval, the sunward and antisunward side of the foreshock often switched sides between Y GSE and -Y GSE, due to changes in the IMF. Because the incident population of electrons is different between the two wings of the foreshock, it is necessary to determine which wing the spacecraft is in for each measurement, requiring an accurate model of the bow shock position. For this study, the shock standoff distance in the X GSE direction is determined using the formula described by *Chapman and Cairns* [2003]. The shock position is then computed according to the hyperbolic model of *Slavin and Holzer* [1981], scaled using the calculated standoff distance, with a focus offset of 3 R_E and an eccentricity of 1.15. A straight IMF line approximation is then used to calculate whether the spacecraft is in the sunward or antisunward foreshock wing. The position of the spacecraft in the foreshock is recalculated for each magnetometer observation.

[15] The statistical imaging results of *Kasaba et al.* [2000] show Langmuir waves activity concentrated tightly around the tangent field line, supporting the validity of the straight IMF approximation within about 30 R_E from the shock. Farther from the shock, this approximation becomes less valid. The study of *Greenstadt et al.* [1995], which measured foreshock activity up to about 100 R_E, do not show Langmuir wave activity confined to the region close to the tangent field line. This result may be explained by variation in the direction of the upstream IMF. For this particular study interval, distant foreshock observations beyond 30 R_E from the shock always correspond to times when the spacecraft is in front of the shock nose in the X GSE direction and necessarily in the sunward wing.

[16] An example day of data is shown in Figure 2. Figure 2a shows a electric field spectrogram measured by the *Wind*/WAVES Thermal Noise Receiver (TNR). The plasma line is apparent as a narrowband feature at around 20 kHz, drifting with variation of the local electron density. The electric field spectrum for each TNR measurement is analyzed according to the method used by *Salem et al.* [2001], which yields an accurate measurement of the plasma frequency. The power near the plasma line is estimated by summing over several frequency bins in the vicinity of the plasma peak. The boundaries of the summation are shown by the white lines on the spectrogram. Figure 2b shows a plot of power near the plasma line, normalized to a level representing the background thermal noise. Langmuir waves are apparent as the bursty increases in the plasma line power. On this example day, significant clusters of strong Langmuir waves occur at around 0500 and 0800 UT, with smaller bursts scattered throughout the remainder of the day.

[17] Figure 2c shows pitch angle distributions for 175–370 eV electrons, measured by the 3DP low energy electron electrostatic analyzer (EESA-L). The relevant electron populations in this energy range are the halo and strahl. The
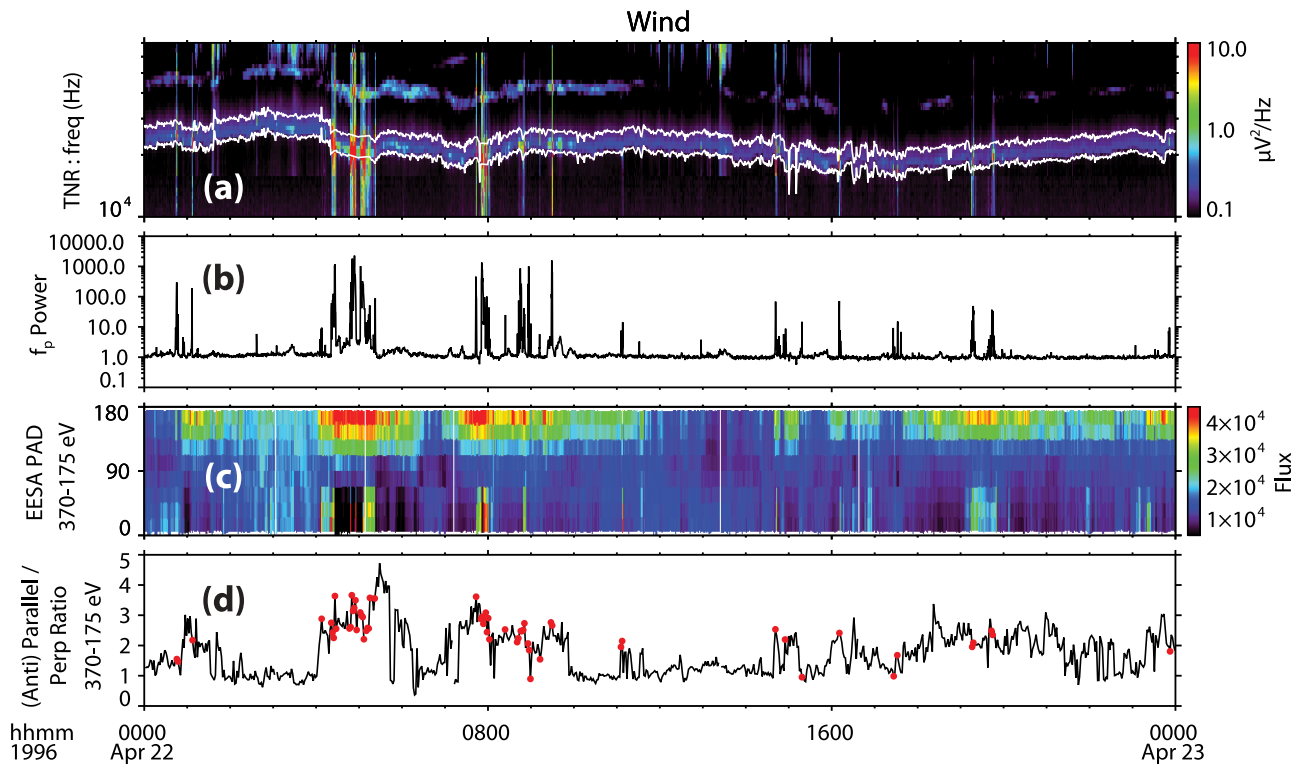
Figure 2. Electron foreshock observations from the *Wind* spacecraft. From top to bottom, the quantities plotted are: (a) the electric field spectrum from the TNR instrument, showing the plasma line and enhancements corresponding to Langmuir wave emission, (b) the normalized power near the plasma line, (c) a pitch angle distribution (in units of flux, $1/sec/cm^2/ster/eV$) of suprathermal electrons, showing the strahl component as an enhancement in the antiparallel direction, and (d) $f_{\pm\parallel}/f_\perp$, the ratio of the parallel (or antiparallel, depending on the magnetic field) electron flux to the perpendicular flux. Red circles indicate regions corresponding to enhanced power near the plasma line signifying Langmuir wave activity. The red circles occur predominantly at times when the strahl is prominent.

strahl is apparent in the sunward-directed pitch angle bins, which on this date are predominantly in the direction antiparallel to the IMF. (Exceptions include the time interval at the very beginning of the day and an interval of several hours around noon.) Foreshock electron beams are evident as brief enhancements in the angular bins near to the IMF-parallel direction. As expected, the beams correspond to times of Langmuir wave activity. Figure 2d shows the ratio of 175–370 eV electron flux in the antiparallel or parallel pitch angle bins (defined by the pitch angles 0°–45° or 135°–180°, depending on IMF direction) to the electrons in the perpendicular bins (defined by the pitch angles 65°–115°). The selection of antiparallel or parallel depends on the direction of the IMF—the parallel quantity in the ratio always represents the incident electrons. This quantity will hereby be referred to as $f_{\pm\parallel}/f_\perp$, the (anti)parallel to perpendicular flux ratio. Each electron measurement which corresponds to a Langmuir wave observation is marked with a red circle. The Langmuir wave observations in Figure 2 occur mainly during times when the strahl is prominent.

3. Analysis

[18] The correlation noted in the previous paragraph can be confirmed statistically using data from the entire interval from 15 March to 24 May. The statistical results are shown in Figure 3. Figure 3 includes two plots, one for the sunward wing of the electron foreshock and one for the antisunward wing. For each plot, the black line shows a histogram of $f_{\pm\parallel}/f_\perp$ for all electron observations. The total number of observations is noted in the axis at the left of the plot. The red line shows a histogram of $f_{\pm\parallel}/f_\perp$ for the subset of electron measurements which occurred during times of Langmuir wave activity. The number of such observations is noted on the red axis at the right of the plot. The scales of the two y-axes have been adjusted so that the area under each curve is equivalent.

[19] Figure 3 (left) represents data from the sunward wing of the foreshock. In the sunward wing, the overall distribution of $f_{\pm\parallel}/f_\perp$ exhibits a double peak. The first and highest peak is at $f_{\pm\parallel}/f_\perp$ slightly higher than 1. This peak represents eVDFs whose suprathermal component is dominated by the halo, which is usually fairly close to isotropic [*Štverák et al.*, 2008]. The second peak at higher values represents the eVDFs with a strong strahl. The histogram for distributions with Langmuir waves shows a single peak at value of $f_{\pm\parallel}/f_\perp$ corresponding to a strong strahl. This shows that, in the sunward foreshock wing, a strong strahl leads to a higher incidence of Langmuir wave activity.

[20] Figure 3 (right) shows data from the antisunward foreshock wing. Because incident electrons in the antisunward wing arrive from the antisunward direction, the beam
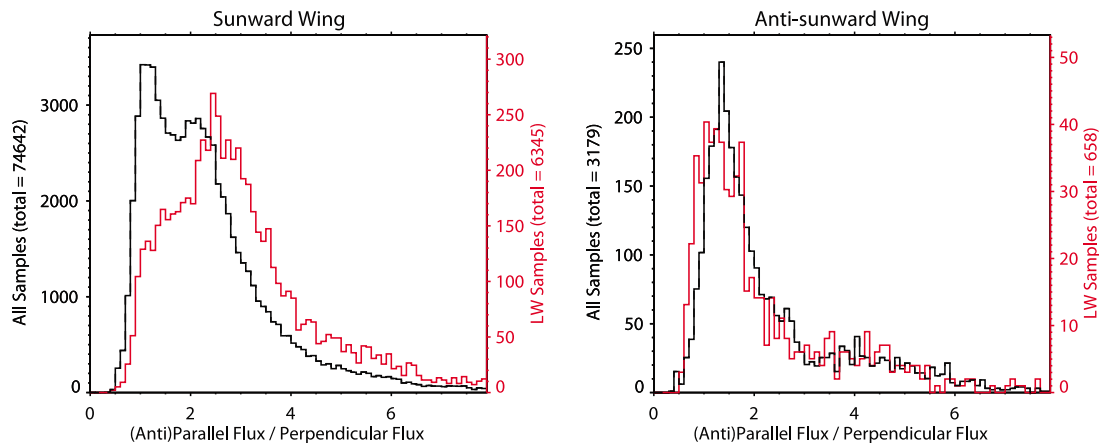
Figure 3. Histograms of the ratio of $f_{\pm\parallel}/f_\perp$, the (anti) parallel flux to perpendicular flux observed by *Wind* from 1996 March 15 to 1996 May 24. (left) Data from the times when *Wind* was in the sunward wing of the bow shock, and (right) data from the time when the spacecraft was in the anti-sunward wing. The black line shows the histogram for all electron observations, while the red line shows the histogram for observations during times of Langmuir wave activity. The histograms have been scaled so that the area under each curve is the same. Incident electrons from the sunward wing of the electron foreshock display a double-peaked distribution, with the peak at higher values of $f_{\pm\parallel}/f_\perp$ being due to the strahl electrons. The histogram of electron observations with concurrent Langmuir wave activity is weighted significantly towards the distributions with higher $f_{\pm\parallel}/f_\perp$, showing that a strong strahl component leads to a significant enhancement in upstream wave activity. In the anti-sunward wing, the incident electrons are from the more isotropic halo population, and $f_{\pm\parallel}/f_\perp$ is unimportant for the generation of Langmuir waves.

consists of reflected halo electrons and the strahl does not play a role. The black line representing the overall distribution shows no double peak, and the two distributions of $f_{\pm\parallel}/f_\perp$ are very similar. It is therefore likely that the generation of electron beams and Langmuir waves in the anti-sunward wing is determined by the magnetic geometry of the shock and is not significantly affected by anisotropy of the upstream eVDF.

[21] We note that a higher percentage of anti-sunward electron observations contain Langmuir waves, despite the fact that there is no strahl present to create the enhancement observed in the sunward wing. This is likely due to the fact that the anti-sunward observations were all made while the spacecraft was relatively close to the Earth, while the sunward observations are made over a range of distances, and Langmuir wave activity decreases with distance from the shock [*Kasaba et al.*, 2000]. This may be the reason why the previous statistical mapping studies of the terrestrial foreshock [*Greenstadt et al.*, 1995; *Kasaba et al.*, 2000] did not report significant asymmetries—the effect of the strahl population may be clearly apparent only when the occurrence is plotted as a function of observed eVDF properties. Nevertheless, there may indeed be some evidence of asymmetry in the results of *Kasaba et al.* [2000], particularly evident in Figure 6 of *Kasaba et al.* [2000]. Figure 6 of *Kasaba et al.* [2000] used the Diff-Dist coordinate system introduced by *Filbert and Kellogg* [1979], in which negative values of Dist correspond to the sunward wing of the foreshock. Figure 6 (middle) of *Kasaba et al.* [2000] shows that for Parker-like IMF conditions, the sunward wing of the foreshock contained higher levels of radio emission, Langmuir waves, and electrons. However, as noted by *Kasaba et al.* [2000], any asymmetry present in the observations is much less obvious than the asymmetry in the Venus foreshock. The clear asymmetry reported at

Venus by *Crawford et al.* [1998] can be explained by the fact that the strahl is much denser relative to the halo in the inner heliosphere than at 1 AU [*Štverák et al.*, 2009].

[22] Previous models for terrestrial foreshock emission, which treat the solar wind eVDF as the sum of a core and halo distribution without accounting for the strahl, predict similar profiles of Langmuir wave electric fields and radio emissivity for the two wings of the electron foreshock, with some slight asymmetry due to the magnetic geometry [*Kuncic et al.*, 2004]. It is likely that taking the strahl population into account will lead to a much larger difference between emissivity between the two wings when the strahl is prominent.

[23] The solar wind speed during the study interval ranged from 300 to 600 km/s, with typical speeds of about 400 km/s. These are typical slow solar wind conditions for low heliographic latitudes during solar minimum, when the solar wind is well ordered into slow regions near the heliographic equator and fast regions near the poles [*McComas et al.*, 2003]. During solar maximum, fast wind occurs at all heliographic latitudes, including the low latitudes near the bow shock. This is significant because the strahl component is of greater prominence in the fast wind than in the slow wind [*Pilipp et al.*, 1987]. The asymmetry between the foreshock wings, already noticeable at solar minimum, may increase substantially in importance during solar maximum.

[24] The mechanism behind the enhancement in Langmuir wave activity was proposed by *Crawford et al.* [1998] and can be described by considering the necessary conditions for beam-driven wave growth. The free energy available for wave growth is determined by the height of the bump on the tail of the electron distribution resulting from the injection of an electron beam into an upstream electron population. In the case where the upstream halo density is much larger than the strahl density, the bump on tail consists of a reflected

halo beam generating a relatively small bump on the tail of the halo distribution. In the case where the upstream strahl density is much larger than the halo density, the bump on tail consists of a reflected strahl beam on top of the small upstream halo tail. The bump on tail would then be quite large and would result in a higher level of Langmuir wave activity. The proposed mechanism is illustrated in Figure 7 of *Crawford et al.* [1998]. This mechanism is possibly similar to the mechanism behind the correlation between strahl electrons and Langmuir waves in solar wind magnetic holes, which has been observed by *Briand et al.* [2010]. A detailed description of the acceleration mechanism and an application to a case study of a single event will be the subject of a follow-up study.

[25] A part of this study interval has been examined previously [*Bale et al.*, 1998, 2000] and evidence was found of a transverse component present in some of the Langmuir waves, which was interpreted as the presence of z-mode waves. Recent observations of Type III radio bursts [*Malaspina et al.*, 2011] indicate that the appearance of transverse components is related to electron beam speed. Given the results of this letter, it is possible that the appearance of transverse components in the electron foreshock is influenced by the presence of the electron strahl.

[26] Finally, we note that the dependence of wave activity on the strahl is an important difference between electron acceleration at bow shocks and at IP shocks. It is conceivable that the mechanism works in reverse for IP shocks—that is, the presence of a strong strahl upstream of an IP shock provides an enhanced tail, which makes it more difficult for the reflected halo electrons to create a bump on tail eVDF.

References

Anderson, K. A., R. P. Lin, F. Martel, C. S. Lin, G. K. Parks, and H. Rème (1979), Thin sheets of energetic electrons upstream from the Earth's bow shock, *Geophys. Res. Lett.*, *6*, 401–404, doi:10.1029/GL006i005p00401.

Bale, S. D., P. J. Kellogg, K. Goetz, and S. J. Monson (1998), Transverse z-mode waves in the terrestrial electron foreshock, *Geophys. Res. Lett.*, *25*, 9–12, doi:10.1029/97GL03493.

Bale, S. D., D. E. Larson, R. P. Lin, P. J. Kellogg, K. Goetz, and S. J. Monson (2000), On the beam speed and wavenumber of intense electron plasma waves near the foreshock edge, *J. Geophys. Res.*, *105*, 27,353–27,367, doi:10.1029/2000JA900042.

Bougeret, J.-L., et al. (1995), Waves: The radio and plasma wave investigation on the Wind spacecraft, *Space Sci. Rev.*, *71*, 231–263, doi:10.1007/BF00751331.

Briand, C., J. Soucek, P. Henri, and A. Mangeney (2010), Waves at the electron plasma frequency associated with solar wind magnetic holes: STEREO/Cluster observations, *J. Geophys. Res.*, *115*, A12113, doi:10.1029/2010JA015849.

Cairns, I. H. (1987), The electron distribution function upstream from the Earth's bow shock, *J. Geophys. Res.*, *92*, 2315–2327, doi:10.1029/JA092iA03p02315.

Cairns, I. H., and P. A. Robinson (1999), Strong evidence for stochastic growth of Langmuir-like waves in Earth's foreshock, *Phys. Rev. Lett.*, *82*, 3066–3069, doi:10.1103/PhysRevLett.82.3066.

Chapman, J. F., and I. H. Cairns (2003), Three-dimensional modeling of Earth's bow shock: Shock shape as a function of Alfvén Mach number, *J. Geophys. Res.*, *108*(A5), 1174, doi:10.1029/2002JA009569.

Crawford, G. K., R. J. Strangeway, and C. T. Russell (1998), Statistical imaging of the Venus foreshock using VLF wave emissions, *J. Geophys. Res.*, *103*, 11,985–12,003, doi:10.1029/97JA02883.

Ergun, R. E., et al. (1998), Wind spacecraft observations of solar impulsive electron events associated with solar type III radio bursts, *Astrophys. J.*, *503*, 435, doi:10.1086/305954.

Filbert, P. C., and P. J. Kellogg (1979), Electrostatic noise at the plasma frequency beyond the Earth's bow shock, *J. Geophys. Res.*, *84*, 1369–1381, doi:10.1029/JA084iA04p01369.

Fitzenreiter, R. J., A. F. Viñas, A. J. Klimas, R. P. Lepping, M. L. Kaiser, and T. G. Onsager (1996), Wind observations of the electron foreshock, *Geophys. Res. Lett.*, *23*, 1235–1238, doi:10.1029/96GL00826.

Greenstadt, E. W., G. K. Crawford, R. J. Strangeway, S. L. Moses, and F. V. Coroniti (1995), Spatial distribution of electron plasma oscillations in the Earth's foreshock at ISEE 3, *J. Geophys. Res.*, *100*, 19,933–19,939, doi:10.1029/95JA01400.

Kasaba, Y., H. Matsumoto, Y. Omura, R. R. Anderson, T. Mukai, Y. Saito, T. Yamamoto, and S. Kokubun (2000), Statistical studies of plasma waves and backstreaming electrons in the terrestrial electron foreshock observed by Geotail, *J. Geophys. Res.*, *105*, 79–103, doi:10.1029/1999JA900408.

Krauss-Varban, D., D. Burgess, and C. S. Wu (1989), Electron acceleration at nearly perpendicular collisionless shocks: 1. One-dimensional simulations without electron scale fluctuations, *J. Geophys. Res.*, *94*, 15,089–15,098, doi:10.1029/JA094iA11p15089.

Kuncic, Z., I. H. Cairns, and S. Knock (2002), Analytic model for the electrostatic potential jump across collisionless shocks, with application to Earth's bow shock, *J. Geophys. Res.*, *107*(A8), 1218, doi:10.1029/2001JA000250.

Kuncic, Z., I. H. Cairns, and S. A. Knock (2004), A Quantitative model for terrestrial foreshock radio emissions: 1. Predicted properties, *J. Geophys. Res.*, *109*, A02108, doi:10.1029/2003JA010125.

Larson, D. E., et al. (1996), Probing the Earth's bow shock with upstream electrons, *Geophys. Res. Lett.*, *23*, 2203–2206, doi:10.1029/96GL02382.

Lefebvre, B., S. J. Schwartz, A. F. Fazakerley, and P. Décréau (2007), Electron dynamics and cross-shock potential at the quasi-perpendicular Earth's bow shock, *J. Geophys. Res.*, *112*, A09212, doi:10.1029/2007JA012277.

Leroy, M. M., and A. Mangeney (1984), A theory of energization of solar wind electrons by the Earth's bow shock, *Ann. Geophys.*, *2*, 449–456.

Lin, R. P., et al. (1995), A three-dimensional plasma and energetic particle investigation for the Wind spacecraft, *Space Sci. Rev.*, *71*, 125–153, doi:10.1007/BF00751328.

Maksimovic, M., V. Pierrard, and P. Riley (1997), Ulysses electron distributions fitted with Kappa functions, *Geophys. Res. Lett.*, *24*, 1151–1154, doi:10.1029/97GL00992.

Maksimovic, M., et al. (2005), Radial evolution of the electron distribution functions in the fast solar wind between 0.3 and 1.5 AU, *J. Geophys. Res.*, *110*, A09104, doi:10.1029/2005JA011119.

Malaspina, D. M., B. Li, I. H. Cairns, P. A. Robinson, Z. Kuncic, and R. E. Ergun (2009), Terrestrial foreshock Langmuir waves: STEREO observations, theoretical modeling, and quasi-linear simulations, *J. Geophys. Res.*, *114*, A12101, doi:10.1029/2009JA014493.

Malaspina, D. M., I. Cairns, and R. E. Ergun (2011), Dependence of Langmuir wave polarization on electron beam speed in type III solar radio bursts, *Geophys. Res. Lett.*, doi:10.1029/2011GL047642, in press.

McComas, D. J., H. A. Elliott, N. A. Schwadron, J. T. Gosling, R. M. Skoug, and B. E. Goldstein (2003), The three-dimensional solar wind around solar maximum, *Geophys. Res. Lett.*, *30*(10), 1517, doi:10.1029/2003GL017136.

Meyer-Vernet, N., and C. Perche (1989), Tool kit for antennae and thermal noise near the plasma frequency, *J. Geophys. Res.*, *94*, 2405–2415, doi:10.1029/JA094iA03p02405.

Pilipp, W. G., H. Miggenrieder, M. D. Montgomery, K.-H. Mühlhäuser, H. Rosenbauer, and R. Schwenn (1987), Characteristics of electron velocity distribution functions in the solar wind derived from the Helios plasma experiment, *J. Geophys. Res.*, *92*, 1075–1092, doi:10.1029/JA092iA02p01075.

Pulupa, M. P., S. D. Bale, and J. C. Kasper (2010), Langmuir waves upstream of interplanetary shocks: Dependence on shock and plasma parameters, *J. Geophys. Res.*, *115*, A04106, doi:10.1029/2009JA014680.

Robinson, P. A. (1992), Clumpy Langmuir waves in type III radio sources, *Sol. Phys.*, *139*, 147–163, doi:10.1007/BF00147886.

Salem, C., J.-M. Bosqued, D. E. Larson, A. Mangeney, M. Maksimovic, C. Perche, R. P. Lin, and J.-L. Bougeret (2001), Determination of accurate solar wind electron parameters using particle detectors and radio wave receivers, *J. Geophys. Res.*, *106*, 21,701–21,717, doi:10.1029/2001JA900031.

Slavin, J. A., and R. E. Holzer (1981), Solar wind flow about the terrestrial planets: 1. Modeling bow shock position and shape, *J. Geophys. Res.*, *86*, 11,401–11,418, doi:10.1029/JA086iA13p11401.

Štverák, Š., P. Trávníček, M. Maksimovic, E. Marsch, A. N. Fazakerley, and E. E. Scime (2008), Electron temperature anisotropy constraints

in the solar wind, *J. Geophys. Res.*, *113*, A03103, doi:10.1029/2007JA012733.

Štverák, Š., M. Maksimovic, P. M. Trávníček, E. Marsch, A. N. Fazakerley, and E. E. Scime (2009), Radial evolution of nonthermal electron populations in the low-latitude solar wind: Helios, Cluster, and Ulysses Observations, *J. Geophys. Res.*, *114*, A05104, doi:10.1029/2008JA013883.

Vocks, C., C. Salem, R. P. Lin, and G. Mann (2005), Electron halo and strahl formation in the solar wind by resonant interaction with whistler waves, *Astrophys. J.*, *627*, 540–549, doi:10.1086/430119.

Wu, C. S. (1984), A fast Fermi process: Energetic electrons accelerated by a nearly perpendicular bow shock, *J. Geophys. Res.*, *89*, 8857–8862, doi:10.1029/JA089iA10p08857.

Yuan, X., I. H. Cairns, P. A. Robinson, and Z. Kuncic (2007), Effects of overshoots on electron distributions upstream and downstream of quasi-perpendicular collisionless shocks, *J. Geophys. Res.*, *112*, A05108, doi:10.1029/2006JA011684.

S. D. Bale, M. P. Pulupa, and C. Salem, Space Sciences Laboratory, University of California, 7 Gauss Way, Berkeley, CA 94708, USA. (bale@ssl.berkeley.edu; pulupa@ssl.berkeley.edu; salem@ssl.berkeley.edu)